Materials Chemistry and Physics 302 (2023) 127722

Contents lists available at ScienceDirect

Materials Chemistry and Physics

journal homepage: www.elsevier.com/locate/matchemphys

Microstructure and magnetization study of Li and Li–Zn ferrites synthesized by an electron beam

Elena N. Lysenko [a], Vitaly A. Vlasov [a,*], Evgeniy V. Nikolaev [a], Anatoliy P. Surzhikov [a], Mikhail V. Korobeynikov [b]

[a] National Research Tomsk Polytechnic University, Tomsk, Russia
[b] Budker Institute of Nuclear Physics SB RAS, Novosibirsk, Russia

HIGHLIGHTS

- Along with conventional thermal annealing the method of heating the initial reagents by fast 2.4 MeV electron beam was used.
- A higher rate of ferrite formation under radiation-thermal conditions was found.
- The saturation magnetization of samples synthesized by electron beam is higher than of thermal synthesized samples.
- The ferrite phases are formed significantly faster in compacted samples.

ARTICLE INFO

Keywords:
Ferrimagnet
Lithium ferrite
Lithium-zinc ferrite
Radiation-thermal synthesis
Electron beam heating
Magnetization

ABSTRACT

Lithium ferrites are widely used in high frequency electronic devices. The present work reports structural and magnetization analysis of lithium ($Li_{0.5}Fe_{2.5}O_4$) and lithium-zinc ($Li_{0.4}Fe_{2.4}Zn_{0.2}O_4$) ferrites synthesized by electron beam heating (RT) of powdered and compacted samples. The synthesis was carried out at 600 and 750 °C for up to 120 min using 2.4 MeV electron beam generated by an ILU-6 pulsed electron accelerator. The characteristics of the samples synthesized by RT were compared with the ones of samples obtained by traditional thermal heating under the same temperature and time conditions. From XRD and thermomagnetometric analyses, α-$Li_{0.5}Fe_{2.5}O_4$ ordered spinel phase and $Li_{0.5(1-x)}Fe_{2.5-0.5x}Zn_xO_4$ ferrite phase with different zinc substitution were formed from Fe_2O_3/Li_2CO_3 and Fe_2O_3/Li_2CO_3/ZnO reagents, respectively. RT synthesis significantly increases the rate of interaction between the initial powders and, as a consequence, the rate of ferrite phase formation. In this case, lithium-containing ferrites can be successfully achieved from compacted powders at 750 °C, which is lower than the temperature of synthesis in conventional thermal heating. The average crystallite sizes calculated from the XRD and BET analyses were 114 nm for Li, 120 nm for Li–Zn ferrites and 142 for Li, 150 nm for Li–Zn, respectively. The specific saturation magnetization and Curie temperature were estimated and are 60 emu/g for Li, 70 emu/g for Li–Zn ferrites and 632 °C for Li, 492 °C for Li–Zn ferrites, respectively. The data obtained in this work are of considerable interest for the creation of a technology for producing ferrites at low synthesis temperatures.

1. Introduction

Ferrites are materials that combine excellent electrical and magnetic properties, including high electrical resistance and magnetization, various hysteresis loops, etc. [1]. Therefore, ferrites are widely used in the electromagnetic field for the manufacture of various devices, such as a phase shifter, circulator, insulator, and so on [2]. Biomedicine has recently become one of the most promising and actively developing areas of ferrites application, including Zn-containing ferrites [3,4].

Magnetically soft lithium ferrites with spinel structure are of particular interest for science and technology. These ferrites exhibit high initial magnetic permeability and saturation magnetization, and low coercive force [5–9]. Unsubstituted lithium (Li) ferrite with the chemical composition of $Li_{0.5}Fe_{2.5}O_4$ is characterized by a rectangular hysteresis loop, the highest Curie temperature and a high saturation magnetization, which makes it possible to use it as a magnetic material

* Corresponding author.
E-mail address: vlvitan75@mail.ru (V.A. Vlasov).

https://doi.org/10.1016/j.matchemphys.2023.127722
Received 7 July 2022; Received in revised form 30 March 2023; Accepted 3 April 2023
Available online 5 April 2023

Table 1
Concentration of spinel phases (C_{spinel}), lattice parameter (a), crystallite size (L), microstrain (Δd/d), X-ray density (ρ_X) and volume of unit cell (V) for Li ferrite samples synthesized at 600 °C.

Sample	C_{spinel} (wt.%)	a (Å)	L (nm)	Δd/ $d{\cdot}10^3$	ρ_X (g/ cm^3)	V (Å)
T_600_0_powder	–	–	–	–	–	–
T_600_10_powder	–	–	–	–	–	–
T_600_20_powder	2.2	8.3250	82	0.7	4.767	576.97
T_600_30_powder	6.7	8.3258	89	0.5	4.765	577.14
T_600_60_powder	14.3	8.3263	84	0.3	4.764	577.24
T_600_120_powder	21.8	8.3267	71	0.2	4.764	577.32
RT_600_0_powder	1.0	8.3245	60	0.6	4.767	576.89
RT_600_10_powder	12.3	8.3248	62	0.5	4.767	576.93
RT_600_20_powder	18.3	8.3253	70	0.5	4.766	577.03
RT_600_30_powder	27.8	8.3262	82	0.3	4.765	577.22
RT_600_60_powder	43.2	8.3270	91	0.4	4.763	577.39
RT_600_120_powder	64.9	8.3277	90	0.3	4.762	577.53
T_600_0_compact	–	–	–	–	–	–
T_600_10_compact	–	–	–	–	–	–
T_600_20_compact	4.3	8.3283	85	0.5	4.761	577.66
T_600_30_compact	10.9	8.3280	69	0.7	4.762	577.59
T_600_60_compact	24	8.3299	75	0.4	4.758	577.99
T_600_120_compact	39.1	8.3330	70	0.2	4.753	578.63
RT_600_0_compact	1.3	8.3257	70	1.5	4.765	577.11
RT_600_10_compact	25.0	8.3287	73	0.3	4.760	577.74
RT_600_20_compact	34.4	8.3296	75	0.5	4.759	577.93
RT_600_30_compact	42.2	8.3296	82	0.1	4.759	577.93
RT_600_60_compact	53.1	8.3307	92	0.3	4.762	577.53
RT_600_120_compact	74.0	8.3320	95	0.1	4.762	577.55

Table 2
Concentration of spinel phases (C_{spinel}), lattice parameter (a), crystallite size (L), microstrain (Δd/d), X-ray density (ρ_X) and volume of unit cell (V) for Li ferrite samples synthesized at 750 °C.

Sample	C_{spinel} (wt.%)	a (Å)	L (nm)	Δd/ $d{\cdot}10^3$	ρ_X (g/ cm^3)	V (Å)
T_750_0_powder	2.2	8.3230	62	0.8	4.770	576.55
T_750_10_powder	27.4	8.3232	74	0.5	4.770	576.60
T_750_20_powder	33.4	8.3241	75	0.7	4.768	576.78
T_750_30_powder	40.1	8.3252	95	0.6	4.766	577.01
T_750_60_powder	51.2	8.3265	126	0.6	4.764	577.28
T_750_120_powder	62.8	8.3277	154	0.5	4.762	577.53
RT_750_0_powder	12.1	8.3290	75	0.1	4.760	577.80
RT_750_10_powder	80.3	8.3295	80	0.1	4.759	577.91
RT_750_20_powder	83.2	8.3296	86	0.3	4.759	577.93
RT_750_30_powder	87.3	8.3295	95	0.5	4.759	577.91
RT_750_60_powder	92.5	8.3298	103	0.4	4.758	577.97
RT_750_120_powder	96.9	8.3299	120	0.7	4.758	577.99
T_750_0_ compact	6.7	8.3213	42	0.8	4.773	576.20
T_750_10_ compact	58.8	8.3300	73	0.4	4.758	578.01
T_750_20_ compact	72.3	8.3302	75	0.3	4.758	578.05
T_750_30_ compact	84.3	8.3305	77	0.2	4.757	578.11
T_750_60_ compact	92.0	8.3306	90	0.2	4.757	578.13
T_750_120_ compact	94.6	8.3350	95	0.2	4.750	579.05
RT_750_0_ compact	92.0	8.3302	36	0.2	4.758	578.05
RT_750_10_ compact	96.5	8.3302	56	0.3	4.758	578.05
RT_750_20_ compact	97.0	8.3305	85	0.5	4.757	578.11
RT_750_30_ compact	98.2	8.3316	102	0.7	4.755	578.34
RT_750_60_ compact	99.1	8.3320	111	1.0	4.755	578.43
RT_750_120_ compact	100	8.3320	114	1.3	4.755	578.43

for transformer cores, antennas, and magnetic recording devices.

Lithium ferrite is often doped with other cations to optimize its electrical and magnetic properties. The introduction of Zn^{2+} ions into lithium ferrite leads to the formation of a substituted lithium-zinc (Li–Zn) ferrite with the chemical composition of $Li_{0.5(1-x)}Fe_{2.5-0.5x}Zn_xO_4$. When $x > 0$, the saturation magnetization of the ferrite increases. However, a decrease in saturation magnetization is observed with increasing Zn^{2+} content at $x \geq 0.4$ [10,11]. Thus, lithium-zinc ferrites are used in high frequency electronic devices (microwave circulators, isolators, phase shifters and absorbers) [12–14].

Table 3
Concentration of spinel phases (C_{spinel}), lattice parameter (a), crystallite size (L), microstrain (Δd/d), X-ray density (ρ_X) and volume of unit cell (V) for Li–Zn ferrite samples synthesized at 600 °C.

Sample	C_{spinel} (wt.%)	a (Å)	L (nm)	Δd/ $d{\cdot}10^3$	ρ_X (g/ cm^3)	V (Å)
T_600_0_powder	–	–	–	–	–	–
T_600_10_powder	–	–	–	–	–	–
T_600_20_powder	1.0	8.3416	74	3.2	4.889	580.43
	–	–	–	–	–	–
T_600_30_powder	1.1	8.3422	63	3.1	4.888	580.55
	1.0	8.3262	80	1.2	4.765	577.22
T_600_60_powder	1.2	8.3418	55	3.0	4.889	580.47
	2.0	8.3265	75	1.2	4.764	577.28
T_600_120_powder	6.0	8.3639	40	2.0	4.850	585.10
	10.0	8.3270	63	0.4	4.763	577.39
RT_600_0_powder	2.0	8.3480	62	1.5	4.878	581.76
	3.0	8.3271	52	1.2	4.763	577.41
RT_600_10_powder	4.0	8.3545	51	0.9	4.867	583.12
	9.7	8.3301	40	1.0	4.758	578.03
RT_600_20_powder	5.2	8.3480	48	1.2	4.878	581.76
	15.2	8.3295	45	0.8	4.759	577.91
RT_600_30_powder	6.2	8.3485	35	1.6	4.877	581.87
	17.3	8.3293	42	1.1	4.759	577.86
RT_600_60_powder	10.3	8.3483	26	2.0	4.878	581.83
	17.4	8.3290	45	0.9	4.760	577.80
RT_600_120_powder	15.1	8.3508	16	2.4	4.873	582.35
	30.0	8.3288	49	0.6	4.760	577.76
T_600_0_compact	–	–	–	–	–	–
T_600_10_compact	2.2	8.3603	60	2.3	4.857	584.34
	0.8	8.3352	80	0.6	4.749	579.09
T_600_20_compact	2.0	8.3593	61	2.8	4.858	584.13
	1.0	8.3346	87	0.8	4.750	578.97
T_600_30_compact	2.4	8.3602	53	1.0	4.857	584.32
	1.7	8.3340	64	0.5	4.751	578.84
T_600_60_compact	10.7	8.3439	66	2.5	4.885	580.91
	6.7	8.3352	74	1.0	4.749	579.09
T_600_120_compact	13.0	8.3552	52	2.8	4.866	583.27
	7.9	8.3364	88	0.8	4.747	579.34
RT_600_0_compact	9.3	8.3456	65	0.9	4.882	581.26
	4.3	8.3352	82	0.7	4.749	579.09
RT_600_10_compact	40.4	8.3523	37	1.4	4.871	582.66
	27.4	8.3347	73	1.0	4.750	578.99
RT_600_20_compact	41.7	8.3641	28	2.0	4.850	585.14
	27.0	8.3289	63	0.2	4.760	577.78
RT_600_30_compact	44.7	8.3593	37	3.6	4.858	584.13
	24.4	8.3287	78	0.6	4.760	577.74
RT_600_60_compact	41	8.3692	40	2.9	4.841	586.21
	29.8	8.3353	66	0.5	4.749	579.11
RT_600_120_compact	43.2	8.3626	46	3.3	4.853	584.82
	29.2	8.3320	81	0.7	4.755	578.43

At present, several methods are employed to produce ferrites with regard to their application, including a sol-gel technology [15–20], citrate precursor and co-precipitation methods [21–23], combustion reaction [24,25], microwave heating, etc. [26,27]. These methods are mainly used to fabricate ferrites with specified, reproducible and uniform electromagnetic properties.

The widespread ceramic method used for producing Li and Li–Zn ferrites employs thermal heating of samples in the furnace [28–31]. This method includes pre-synthesis of ferrite based on solid-phase interaction between the initial oxides (Fe_2O_3, Li_2CO_3 and ZnO) at 800–900°C, and subsequent high-temperature sintering at 1100–1200°C to obtain dense ferrite samples. However, high temperatures used in ceramic technology can cause volatilization of lithium and zinc from samples, violation of the stoichiometric composition of ferrites, and, therefore, decreased electrical resistance and increased dielectric losses.

To reduce the ferrite synthesis temperature, a method of heating the

Table 4
Concentration of spinel phases (C_{spinel}), lattice parameter (a), crystallite size (L), microstrain (Δd/d), X-ray density (ρ_X) and volume of unit cell (V) for Li–Zn ferrite samples synthesized at 750 °C.

Sample	C_{spinel} (wt.%)	a (Å)	L (nm)	Δd/d·10^3	ρ_X (g/cm^3)	V (Å)
T_750_0_powder	–	–	–	–	–	–
T_750_10_powder	7.4	8.3619	34	2.2	4.854	584.68
	13.0	8.3266	54	0.6	4.764	577.30
T_750_20_powder	10.3	8.3615	30	2.5	4.855	584.59
	18.3	8.3282	58	0.8	4.761	577.63
T_750_30_powder	14.2	8.3610	28	2.7	4.855	584.49
	21.3	8.3295	63	1.2	4.759	577.91
T_750_60_powder	22.2	8.3604	24	3.2	4.856	584.36
	25.8	8.3312	73	1.2	4.756	578.26
T_750_120_powder	25.4	8.3602	18	4.1	4.857	584.32
	40.0	8.3345	78	1.4	4.750	578.95
RT_750_0_powder	10.6	8.3562	30	3.2	4.864	583.48
	14.1	8.3354	52	0.9	4.749	579.13
RT_750_10_powder	35.1	8.3556	33	2.7	4.865	583.35
	15.0	8.3362	47	1.2	4.747	579.30
RT_750_20_powder	40.2	8.3562	33	2.8	4.864	583.48
	20.3	8.3375	48	1.1	4.745	579.57
RT_750_30_powder	46.3	8.3580	36	2.5	4.861	583.86
	15.2	8.3384	40	1.5	4.744	579.76
RT_750_60_powder	59.6	8.3589	45	2.2	4.859	584.05
	12.8	8.3395	35	1.8	4.742	579.99
RT_750_120_powder	72	8.3593	51	2.0	4.858	584.13
	11.9	8.3401	38	1.8	4.741	580.11
T_750_0_ compact	15.2	8.3610	36	1.9	4.855	584.49
	33.0	8.3275	73	0.8	4.762	577.49
T_750_10_ compact	28.0	8.3646	22	1.9	4.849	585.24
	31.0	8.3260	80	1.0	4.765	577.18
T_750_20_ compact	47.9	8.3609	45	3.0	4.856	584.47
	20.2	8.3285	75	0.6	4.761	577.70
T_750_30_ compact	60.0	8.3724	40	2.8	4.836	586.88
	15.3	8.3402	26	0.9	4.741	580.14
T_750_60_ compact	66.0	8.3701	42	3.0	4.840	586.40
	14.6	8.3372	14	0.7	4.746	579.51
T_750_120_ compact	82.0	8.3679	46	3.1	4.843	585.94
	11.9	8.3319	83	0.1	4.755	578.41
RT_750_0_ compact	67.8	8.3651	48	2.7	4.848	585.35
	18.2	8.3267	95	0.5	4.764	577.32
RT_750_10_ compact	80.0	8.3629	50	3.0	4.852	584.89
	12.0	8.3309	113	0.4	4.757	578.20
RT_750_20_ compact	83.2	8.3613	57	3.3	4.855	584.55
	11.8	8.3325	20	3.1	4.754	578.53
RT_750_30_ compact	89.4	8.3590	73	1.7	4.859	584.07
	9.6	8.3307	78	0.9	4.757	578.16
RT_750_60_ compact	92.5	8.3582	81	1.3	4.860	583.90
	7.5	8.3312	89	2.1	4.756	578.26
RT_750_120_ compact	100	8.3572	120	1.8	4.862	583.69
	–	–	–	–	–	–

initial reagents by electron beam with energies above 1 MeV was proposed [32–36]. This radiation-thermal (RT) heating technique increases the rate of the solid-phase reaction between the initial reagents due to defect formation induced by electron-beam irradiation. In Refs. [37,38], the X-ray phase analysis was employed to study the kinetic patterns of lithium and lithium-zinc ferrite synthesis by high-energy electron beam heating of initial powders Fe_2O_3–Li_2CO_3 and Fe_2O_3–Li_2CO_3–ZnO, respectively. The kinetic analysis of the dependences of the spinel phase accumulation during ferrite synthesis was performed using a formal kinetic equation. It was found that ferrite formation during RT heating is accelerated due to decreased activation energy for synthesis and a reduced pre-exponential factor in the temperature dependence of ferrite formation.

It is known that during synthesis of lithium-substituted ferrites, transitional spinel phases can be formed, which are difficult to distinguish from the magnetic phase of ferrite of a given composition in X-ray patterns. This complicates identification of ferrites based on X-ray phase data. However, there are characteristics, such as saturation magnetization and Curie temperature, which are not sensitive to microstructure and can be therefore used to estimate the degree of ferritization of the synthesized powders. In this study, these characteristics were used to analyze Li and Li–Zn ferrites synthesized under various conditions. This made it possible to correctly identify the formation of certain ferrite phases during their synthesis by the electron-beam heating.

2. Experimental

To produce lithium $Li_{0.5}Fe_{2.5}O_4$ and lithium-zinc $Li_{0.4}Fe_{2.4}Zn_{0.2}O_4$ ferrites, the initial high pure powders of Fe_2O_3 (91.5 and 86.05 wt%), Li_2CO_3 (8.5 and 6.64 wt%), and ZnO (7.31 wt%) were used. The powders were pre-dried and mixed using an agate mortar. The mixture of initial reagents was divided into two portions. The first one consisted of powder samples with a bulk density of at ca. 1 g/cm^3, and the second one included compacts with a density of 2.6 g/cm^3 obtained by hydraulic pressing at 200 MPa.

RT synthesis of samples was performed at 600 and 750 °C for up to 120 min using an ILU-6 accelerator developed at INP SB RAS (Novosibirsk, Russia). This accelerator generates a pulsed electron beam with electron energy of 2.4 MeV. The pulsed beam current was 400 mA, the pulse duration was 500 μs, and the pulse repetition rate of 12.5 Hz.

The X-ray diffraction (XRD) analysis was performed using an ARL X'TRA (ThermoFisher Scientific) diffractometer with a semiconductor Si (Li) Peltier detector and CuKα radiation. XRD patterns were processed by the full profile analysis using the Powder Cell 2.4 software, where the pseudo-Voigt profile function was used. Phases were identified by the PDF-4+ powder database of the International Center for Diffraction Data (ICDD). The crystallite sizes (L) and microstrain (Δd/d) were calculated by Williamson-Hall's formula using the Powder Cell 2.4 software.

The microstructure of the synthesized ferrites was investigated using a Hitachi TM-3000 scanning electron microscope and a Solver P47 atomic-force microscope. The latter, the microrelief of the samples was examined by the AFM method in a tapping mode. From the Brunauer-Emmett-Teller (BET), the specific surface area for samples was estimated.

Magnetization of the synthesized ferrite was studied via two methods: measurement of the specific saturation magnetization (σ_S) using a magnetometer and thermomagnetometric measurements using a thermal analyzer. The latter, which is based on thermogravimetry in a magnetic field, enables analysis of magnetic phase transitions in samples and determination of their Curie temperature [39–41]. It was performed using a Netzsch STA 449C Jupiter thermal analyzer and corundum crucibles. The samples were heated at the device maximum rate of 50 °C/min to 800 °C in order to reduce the synthesis effect during the analysis of the magnetic phase transition. In the analysis, a thermocouple was used to simultaneously record thermal effects. The obtained thermogravimetric (TG) and calorimetric (DSC) curves were processed using the Netzsch Proteus Analysis software. The thermomagnetometry method is described in more detail in Ref. [42].

3. Results and discussion

Synthesis of lithium and lithium-zinc ferrites proceeds in accordance with the formulae:

$$Li_2CO_3 + 5Fe_2O_3 \rightarrow 4Li_{0.5}Fe_{2.5}O_4 + CO_2 \quad (1)$$

$$Li_2CO_3 + (5-x)(1-x)^{-1}Fe_2O_3 + 4x(1-x)^{-1}ZnO \rightarrow 4(1-x)^{-1}Li_{0.5(1-x)}Fe_{2.5-0.5x}Zn_xO_4 + CO_2 \quad (2)$$

In equation (2), at $x = 0.2$, ferrite of the $Li_{0.4}Fe_{2.4}Zn_{0.2}O_4$ composition is formed during synthesis:

$$Li_2CO_3 + 6Fe_2O_3 + ZnO \rightarrow 5Li_{0.4}Fe_{2.4}Zn_{0.2}O_4 + CO_2 \quad (3)$$

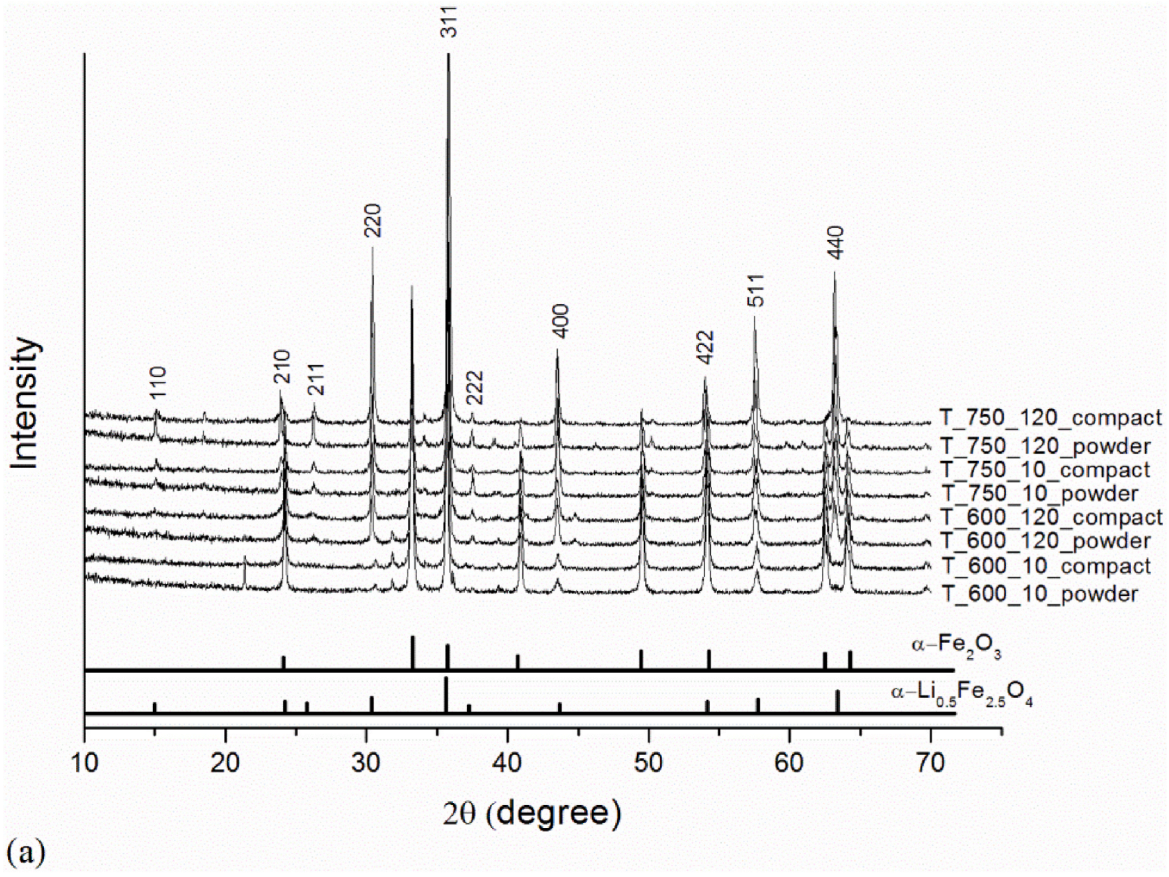

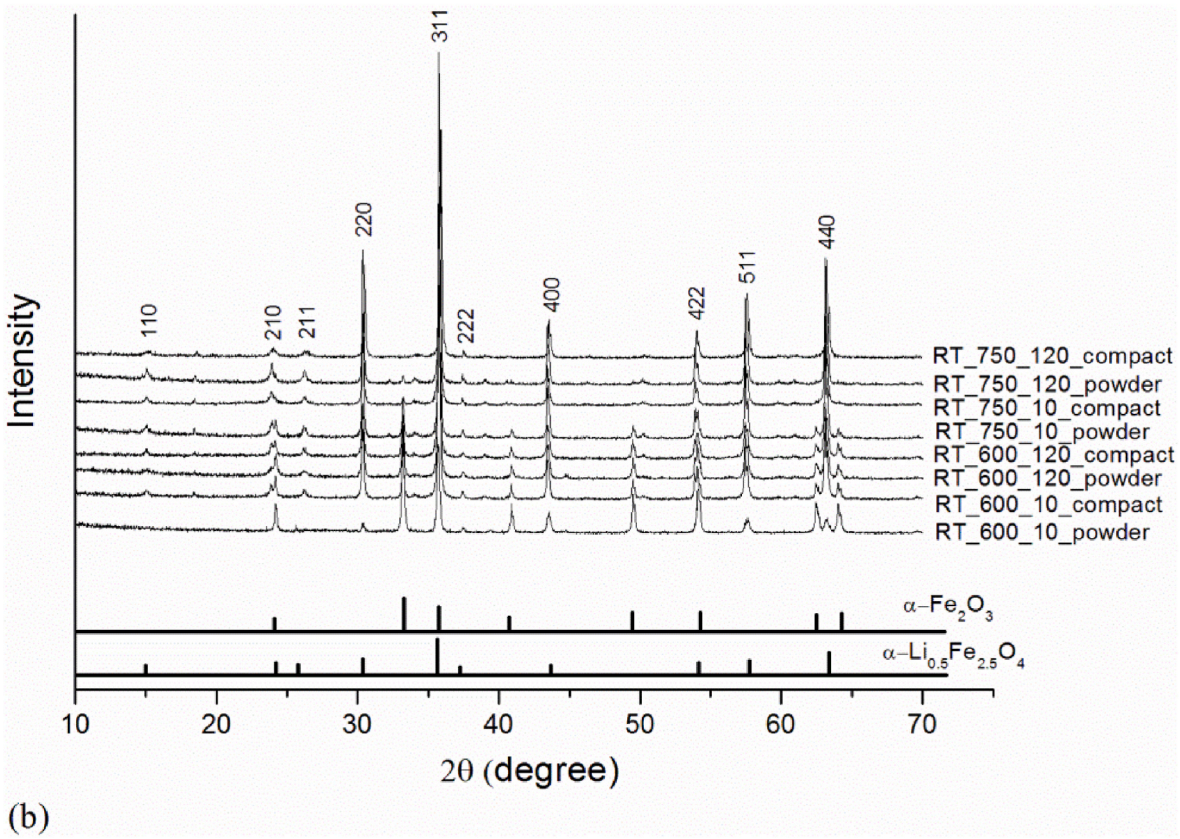

Fig. 1. XRD patterns of Li ferrite synthesized via thermal (a) and electron beam heating (b) at 600 and 750 °C for 10 and 120 min.

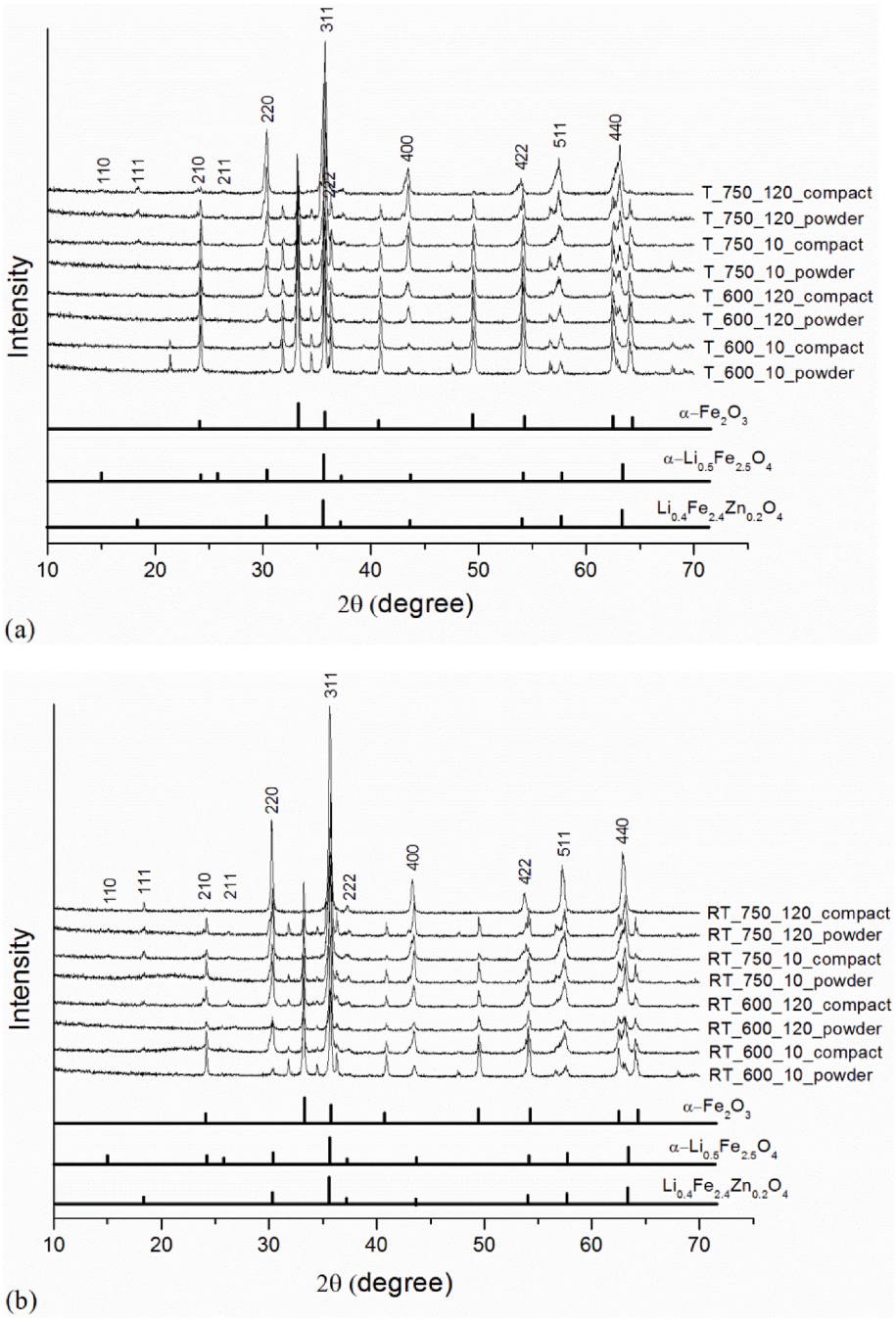

Fig. 2. XRD patterns of Li–Zn ferrite synthesized via thermal (a) and electron beam heating (b) at 600 and 750 °C for 10 and 120 min.

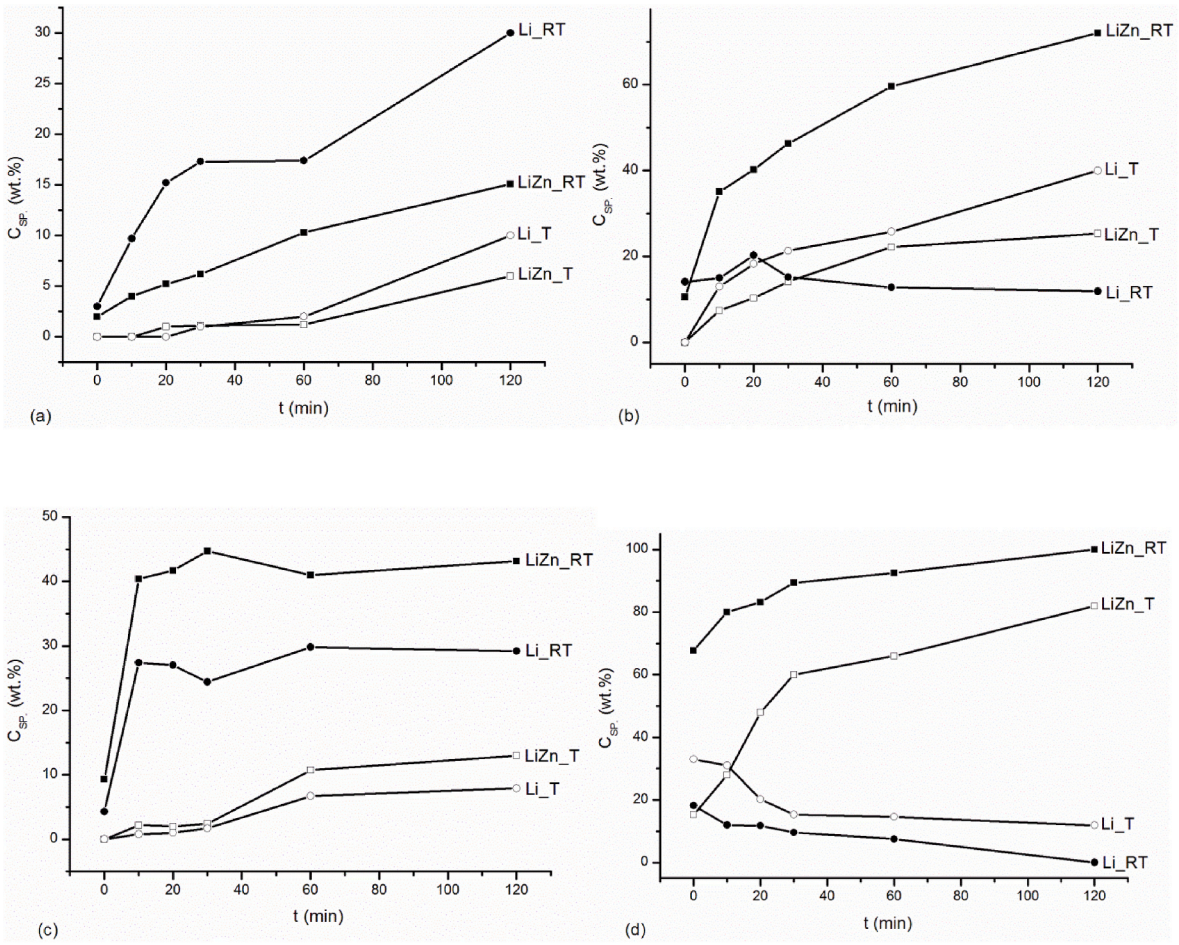

Fig. 3. Variation in concentration of synthesized spinel phases in Li–Zn ferrite at modes: (a) - 600_powder; (b) - 750_powder; (c) - 600_compact; (d) - 750_compact.

The X-ray diffraction patterns obtained for samples synthesized in the temperature range of (600–750) °C were a set of reflections of the initial components phases and the spinel phases associated with formation of lithium ferrites, the content of which depends on temperature and time of synthesis, as well as on the density of the samples. XRD data obtained in all modes are summarized in Tables 1–4.

Fig. 1 shows the XRD patterns of Li ferrite samples synthesized for 10 and 120 min. For samples obtained at 600 °C for up to 10 min, the XRD analysis shows the reflections from the initial component phases as Fe_2O_3. With an increase in temperature and synthesis time (Tables 1 and 2), the content of iron oxide decreases, while the content of ordered α-$Li_{0.5}Fe_{2.5}O_4$ phase (ICDD card no. 00-049-0266) increases both during thermal and electron beam heating. In this case, the lattice parameter of the synthesized lithium ferrite increases, which may be due to an increase in the concentration of Fe^{2+} ions in the spinel lattice of the ferrite. However, the obtained values of the lattice parameter correspond to the research data (0.833 nm) for lithium ferrite [5]. For samples pre-compacted and synthesized by RT, the concentration of lithium ferrite and, consequently, the consumption of iron oxide is much higher than that after thermal heating. This can be observed when comparing individual (non-overlapping) reflections for iron oxide ($2\theta = 33.2°$) and lithium ferrite spinel ($2\theta = 26.2°$).

Fig. 2 shows the XRD patterns of Li–Zn ferrite samples synthesized for 10 and 120 min. The analysis of the samples revealed the presence in them of both remnants of unreacted iron oxide and two spinel phases with different lattice parameters, corresponding to lithium ferrite and lithium-zinc ferrite (Tables 3 and 4). Most likely, during synthesis of Li–Zn ferrite, Li ferrite is formed as a transition phase. Thus, there is a parallel formation of two forms of ferrites in accordance with Eqs. (1) and (3). The change in the concentration of synthesized ferrites with an increase in the synthesis time is shown in Fig. 3. For samples synthesized from powders at 600 °C under the same heating method, a more intense formation of unsubstituted lithium ferrite occurs compared to lithium-zinc ferrite. In other synthesis modes, the concentration of lithium-zinc ferrite is higher, which indicates its formation due to the interaction of the α-$Li_{0.5}Fe_{2.5}O_4$ phase with iron oxide. The lattice parameter of Li–Zn ferrite (ICDD card no. 00-038-0259) synthesized under different modes varies slightly and corresponds to the data (0.836 nm) obtained in Ref. [7].

From the XRD results, it follows that the formation of ferrites during electron-beam heating proceeds at a higher rate than during conventional thermal heating. As can be seen from Fig. 3d (at $t = 0$ min in Figure), a large amount of Li–Zn ferrite (above 60 wt%) is formed during nonisothermal heating by an electron beam at 750 °C in the case of sample compaction. Further, the concentration of ferrite accumulates up to 100 wt% with an increase in the time of isothermal synthesis. In this case, the size of crystallites, estimated from the XRD data, increases to 120 nm (Table 4).

Microstructural analysis was carried out for initial reagents (Fig. 4). The spherical, rod-like and flake-like morphologies were observed from SEM images for Fe_2O_3, Li_2CO_3 and ZnO powders, respectively.

The SEM images shown in Fig. 5 indicate the irregular particles in the synthesized ferrite samples. The samples have a porous structure, which is expected in the case of obtaining ferrites via synthesis at temperatures much lower than the ceramic sintering temperature. The samples obtained by RT of pre-compacted samples have a denser structure. Structure image obtained by the AFM method and shown in Fig. 6 for the Li–Zn ferrite revealed the average particle size of about 290 nm.

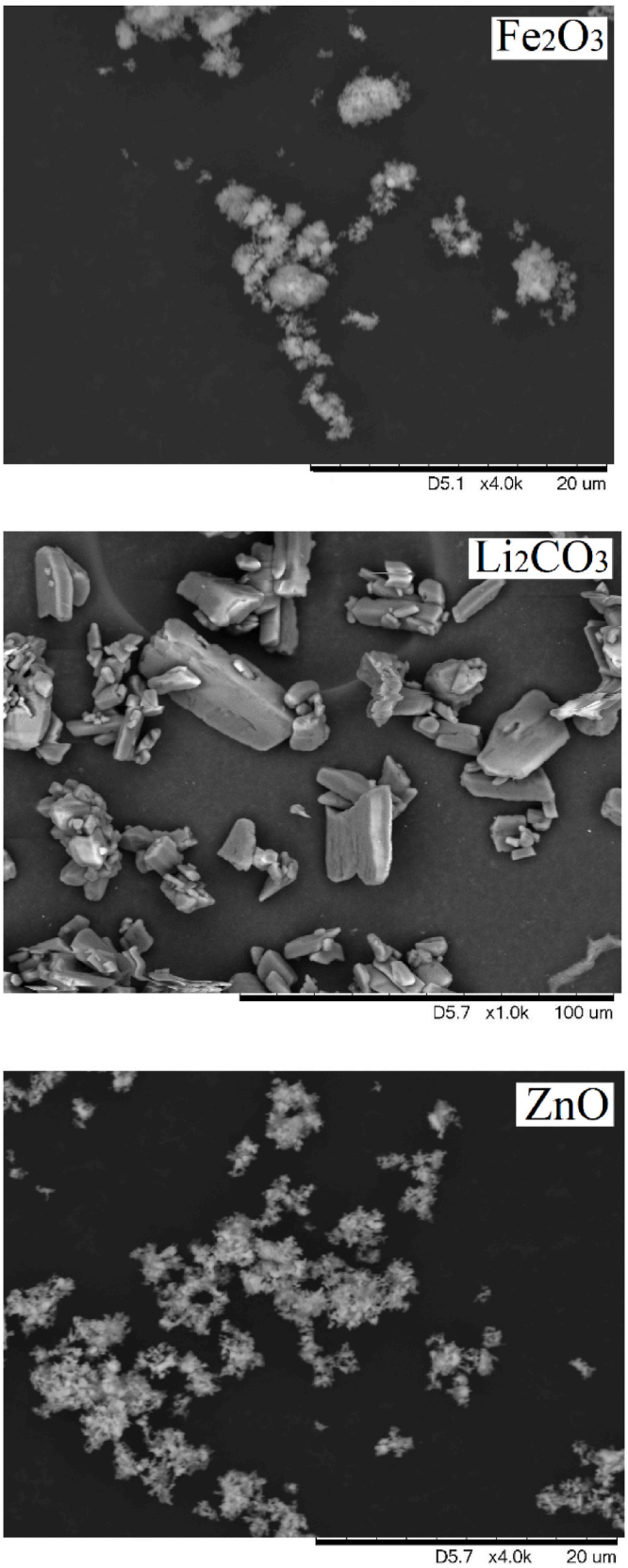

Fig. 4. SEM images of initial reagents.

The BET surface area values were found to be 8.9 and 8.2 m^2/g, respectively, for Li and Li–Zn ferrites synthesized at 750 °C by electron beam heating of compacted samples. These values are in good agreement with previously published values for similar powders [43]. The crystallite size values calculated from the BET analysis are shown in Table 5 and are slightly larger than those obtained from the XRD data.

As mentioned above, the synthesized ferrites are magnetically soft ferrite materials. Magnetization of these ferrites is spontaneous due to the spin magnetic moments of trivalent iron ions and divalent metal ions, which show an indirect exchange interaction through oxygen ions. The coercivity of lithium and lithium-zinc ferrites is low (of the order of 10–20 Oe [44,45]), and when an external magnetic field is applied, they are easily magnetized up to saturation magnetization. In the study, the specific saturation magnetization was measured under an external magnetic field of 4.7 kOe.

The data on the specific magnetization of the samples obtained by measuring are shown in Fig. 7. For both ferrites, the σ_S value increases at increased synthesis time, which indicates the accumulation of the magnetic phase in the samples. In general, the behavior of the specific magnetization of the samples is similar to the pattern of the change in the spinel phase concentration in these samples during their synthesis.

During thermal synthesis at 600 °C (Fig. 7 a,c), magnetization of the samples grows slowly and linearly, which indicates a slow diffusion interaction between the initial oxides with formation of the ferrite phase. Samples synthesized by electron beam show a faster growth of the σ_S value.

The synthesis temperature increased to 750°C accelerates formation of the ferrite magnetic phase. In this case, the samples heated by electron beam exhibit sufficiently high saturation magnetization by the beginning of the isothermal holding stage ($t = 0$ min in Fig. 7 b,d). This indicates a significant concentration of the magnetic phase at the stage of non-isothermal heating of samples. As the isothermal holding time increases, magnetization of the samples increases and becomes stable within 120 min.

In addition, the results revealed a higher degree of specific magnetization of compacted samples compared to powdered samples, which indicates a higher content of the spinel magnetic phase in the synthesized compacts. This is due to the fact that denser compacts provide a high contact area between the particles of the initial reagents and increase the rate of ferrite formation.

The specific magnetization of the samples fabricated from the compacted mixture and those RT-synthesized at 750 °C for 120 min is close to the nominal σ_S values for Li (60 emu/g) [44] and Li-Zi (70 emu/g) [45] ferrites, which indicates a high content of these ferrite phases in the synthesized samples.

Synthesis of Li-substituted ferrites can cause formation of transitional magnetic phases with different degree of magnetization; therefore, the study additionally employed the thermomagnetometric analysis for monitoring the synthesized samples.

Fig. 8 shows the TG and DSC curves for Li ferrite obtained by heating the synthesized samples in a thermal analyzer furnace. At a low synthesis temperature of 600 °C (Fig. 8a), further interaction between the reagents with the release of CO_2 proceeds in the powder samples according to Eq. (1), which is evidenced by reduced weight in the TG curve. Since the theoretical weight reduction due to the total release of CO_2 is 5.04% with a reaction enthalpy of 108–110 J/g [46,47], the observed weight measurement of 1.72% and the thermal effect of 49 J/g correspond to partial synthesis between the residual iron oxide and lithium carbonate according to the thermomagnetometric analysis. This is evidenced by the DSC peak observed at 725 °C, which is related to the decomposition temperature of Li_2CO_3 residues.

For other samples, the TG curve shows an increase in weight in the temperature range of 600–650 °C, which is caused by magnetic phase transition, that is, by magnetic–paramagnetic transition in the synthesized magnetic phase. The peak in the derivative thermogravimetric (DTG) curve indicates the Curie temperature of a given magnetic phase.

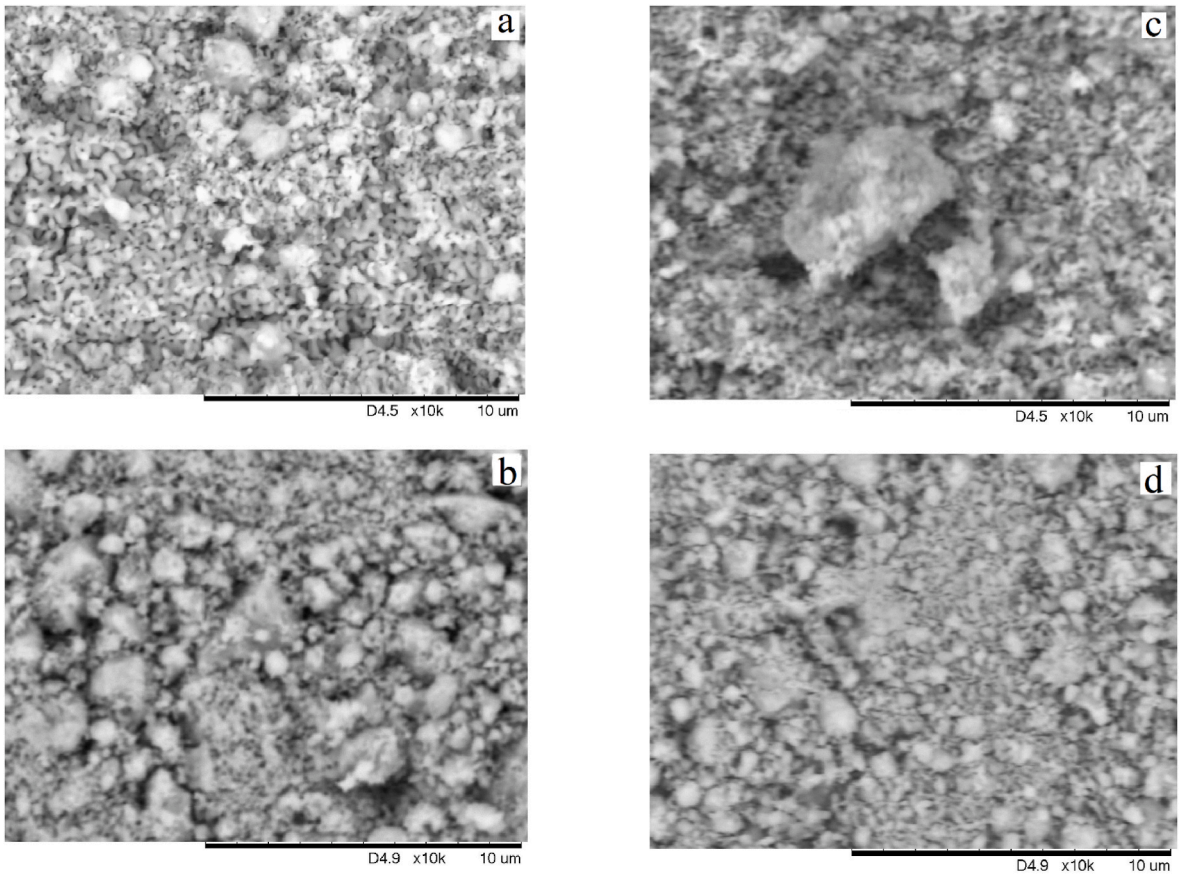

Fig. 5. SEM images of Li (a, b) and Li–Zn (c, d) ferrites synthesized by electron beam at 750°C using powdered samples (a, c) and compacted samples (b, d).

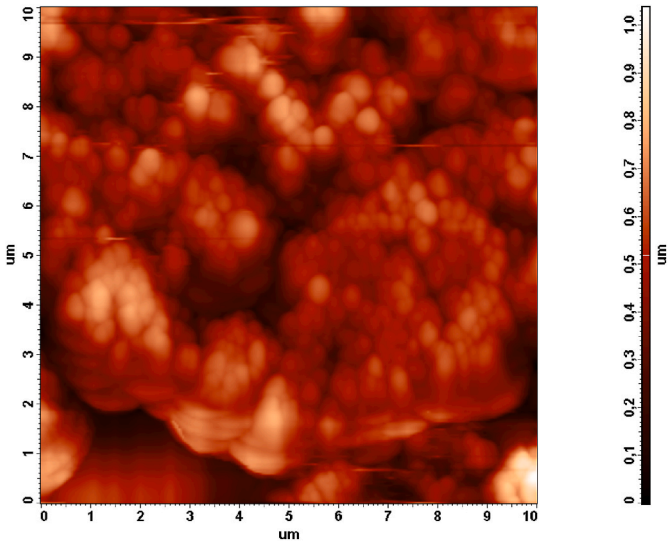

Fig. 6. Structure image obtained by the AFM method for the Li–Zn ferrite synthesized by electron beam at 750°C from compacted sample.

Table 5
Specific surface area and crystallite size from BET analysis.

Composition	S (m^2/g)	D (nm)
Li	8.9	142
Li–Zn	8.2	150

The observed temperatures of 628–633 °C are found to be close to the Curie temperature of lithium ferrite with the chemical formula $Li_{0.5}Fe_{2.5}O_4$ [44,48].

An increased height of the weight jump in the TG curves plotted in Fig. 8 is due to a stronger interaction of the synthesized magnetic phase with an external magnetic field during thermomagnetometric measurements and, hence, with higher magnetization of the sample. The height of the weight jump depends on temperature, heating method, and density of the samples. Higher values of weight jumps can be observed in pre-compacted and RT-synthesized samples, and this indicates a significantly higher content of the magnetic phase. This is also confirmed by an increase in the DSC peak area at 748–762 °C caused by transition of the α−$Li_{0.5}Fe_{2.5}O_4$ phase to the β−$Li_{0.5}Fe_{2.5}O_4$ phase in partially synthesized lithium ferrite. For pure lithium ferrite, the enthalpy of this transition is ~12 J/g [49]. Therefore, the DSC peak area of 8.8 J/g for a compact RT-synthesized within 120 min corresponds to formation of ~73 wt% lithium ferrite during synthesis (Fig. 8h).

Fig. 9 shows TG and DSC curves obtained by thermomagnetometric analysis for Li–Zn ferrite. At 600 °C (Fig. 9a), weight reduction in the TG curve for powder samples is caused by the interaction between non-synthesized reagents followed by the release of CO_2 in accordance with Eq. (2). Since the theoretical weight reduction due to the total release of CO_2 for Li–Zn ferrite is 3.95% with a reaction enthalpy of 70–80 J/g [43,50], thermomagnetometric analysis shows that the observed weight measurement of 1.65% and the thermal effect of 53 J/g correspond to partial synthesis of the residues of Fe_2O_3, Li_2CO_3 and ZnO.

The thermal results obtained in the temperature range of 700–750 °C show that the sample compacted and synthesized at 600 °C (Fig. 8b) contains a significantly smaller amount of residues of the initial reagents. In this case, the TG curve shows an increase in weight in the temperature range of 600–650 °C, which is associated, as shown above,

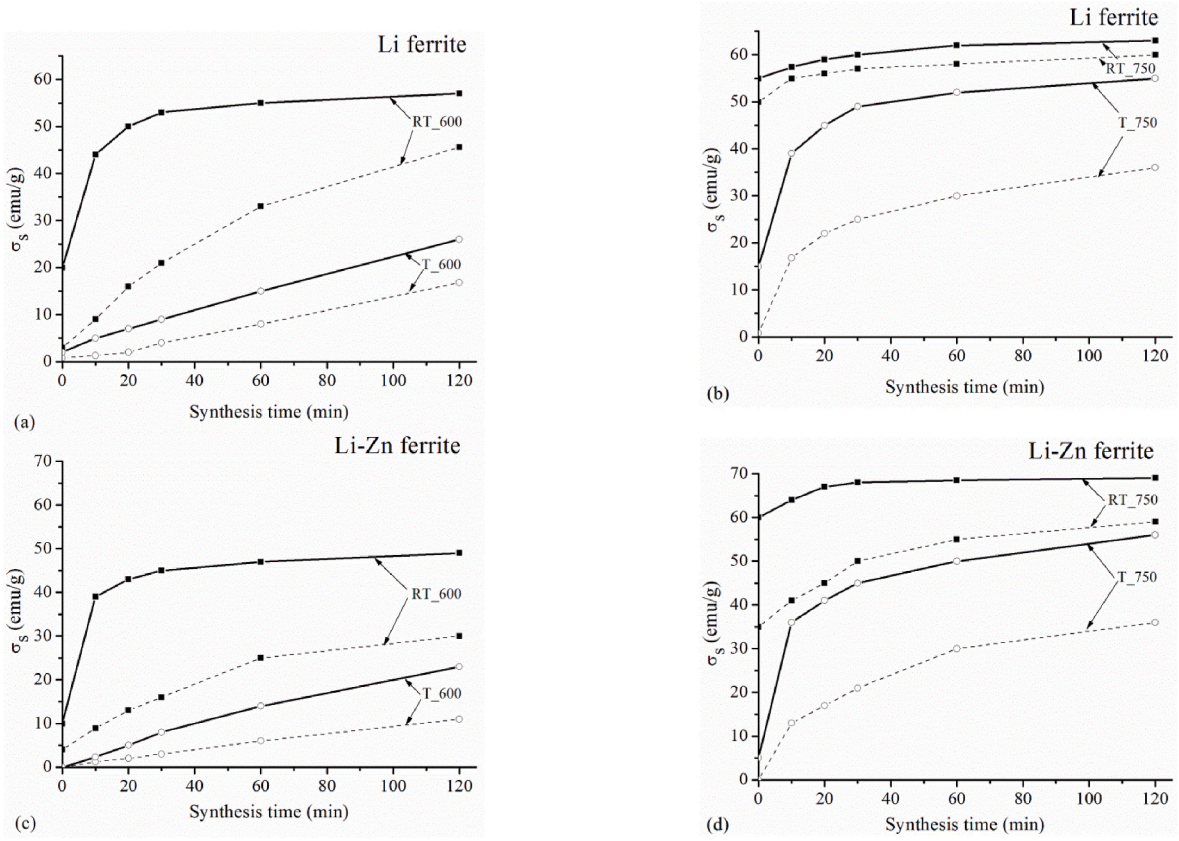

Fig. 7. Kinetic dependences of the specific magnetization of Li (a, b) and Li–Zn (c, d) ferrites synthesized by electron beam (RT samples) and thermal annealing (T samples) at 600 (a, c) and 750 (b, d) °C: lines indicate compacted samples; dotted lines show powdered samples.

with the magnetic phase transition in the synthesized magnetic phase of lithium ferrite $Li_{0.5}Fe_{2.5}O_4$ with a Curie temperature of 622 °C. Li ferrite is apparently formed as a transition phase during synthesis of lithium-zinc ferrite. A significantly higher content of this phase was found in the RT-synthesized compacted samples, which is evidenced by a sharp jump in weight during the magnetic phase transition and a Curie temperature of 631 °C corresponding to the literature data for lithium ferrite and the presence of the DSC peak with an enthalpy of 0.38 J/g at 755 °C (Fig. 8f). It is known that the Curie temperature of lithium-zinc ferrite is 490–500 °C [50]. The TG curve shows no changes in weight in this temperature range for the above samples, which indicates that an increase in the specific saturation magnetization observed in Fig. 7c is due to synthesis of the magnetic phase of pure lithium ferrite, which exhibits lower magnetization compared to that of Li–Zn ferrite [51,52]. A similar pattern of changes in σ_S and its similar values for both ferrites synthesized at 600 °C under thermal heating (Fig. 7a and c) confirm the assumptions made.

At synthesis temperature increased up to 750 °C, the content of Li ferrite decreases, while the content of lithium-substituted zinc phases increases (Fig. 9c,d,g,h). This increase is more significant in compacted samples (Fig. 9d,h). A compacted sample synthesized by thermal heating shows formation of several spinel phases, including the $Li_{0.5}Fe_{2.5}O_4$ ferrite phase and a wide range of $Li_{0.5(1-x)}Fe_{2.5-0.5x}Zn_xO_4$ lithium-substituted ferrite phases with different Curie temperatures corresponding to $x<2$ in the chemical formula. Despite similar thermal data, the sample synthesized by electron beam contains a significant amount of lithium-zinc ferrite with a Curie temperature of 492 °C close to that reported in the literature (Fig. 9h).

Apparently, when the $Fe_2O_3/Li_2CO_3/ZnO$ mixture is heated by electron beam, the rate of the lithium ferrite ($Li_{0.5}Fe_{2.5}O_4$) formation sharply grows at the initial stage of RT synthesis of ferrite. At later stages of synthesis, formation of lithium-zinc phases with different zinc substitution $Li_{0.5(1-x)}Fe_{2.5-0.5x}Zn_xO_4$ and reactions between the initially formed phases can be observed. As a result, solid solutions of spinel ferrites are formed, which is confirmed by thermal analysis.

4. Conclusions

This study aimed to investigate the synthesis of lithium and lithium-zinc ferrites under conditions of thermal and electron-beam heating of samples at low temperatures. It was established that the rate of ferrite formation depends on temperature and time of synthesis, heating method, and density of the samples (powdered and compacted samples). With an increase in temperature from 600 to 750 °C and synthesis time up to 120 min, spinel ferrite phases were found to grow in the samples, which were confirmed by XRD data and magnetization measurements. Moreover, in pre-compacted samples, ferrite phases were formed significantly faster. From XRD, calorimetric and thermomagnetometric analyses, an ordered spinel phase α-$Li_{0.5}Fe_{2.5}O_4$ is synthesized during the heating Fe_2O_3/Li_2CO_3 initial reagents. The synthesis of lithium-zinc ferrite proceeds through the parallel formation of $Li_{0.5}Fe_{2.5}O_4$ and $Li_{0.5(1-x)}Fe_{2.5-0.5x}Zn_xO_4$ ferrite phases during the heating $Fe_2O_3/Li_2CO_3/ZnO$ initial reagents. In the latter case, the weight ratio of synthesized ferrite phases depends on the synthesis mode. Electron-beam heating significantly accelerates the rate of interaction between the $Li_{0.5}Fe_{2.5}O_4$ transition phase and iron oxide residues and, as a result, the rate of formation of substituted by zinc ferrite phases. Thus, lithium-containing ferrites can be successfully achieved by an electron beam heating at 750 °C. This synthesis temperature is lower compared to the temperature of 900 °C used in the case of the synthesis of lithium ferrites by conventional thermal heating. In conclusion, it should be noted that the data obtained in this work are of considerable interest for the creation of a technology for producing ferrites at low synthesis temperatures, which is important in the case of using volatile components in the initial ferrite

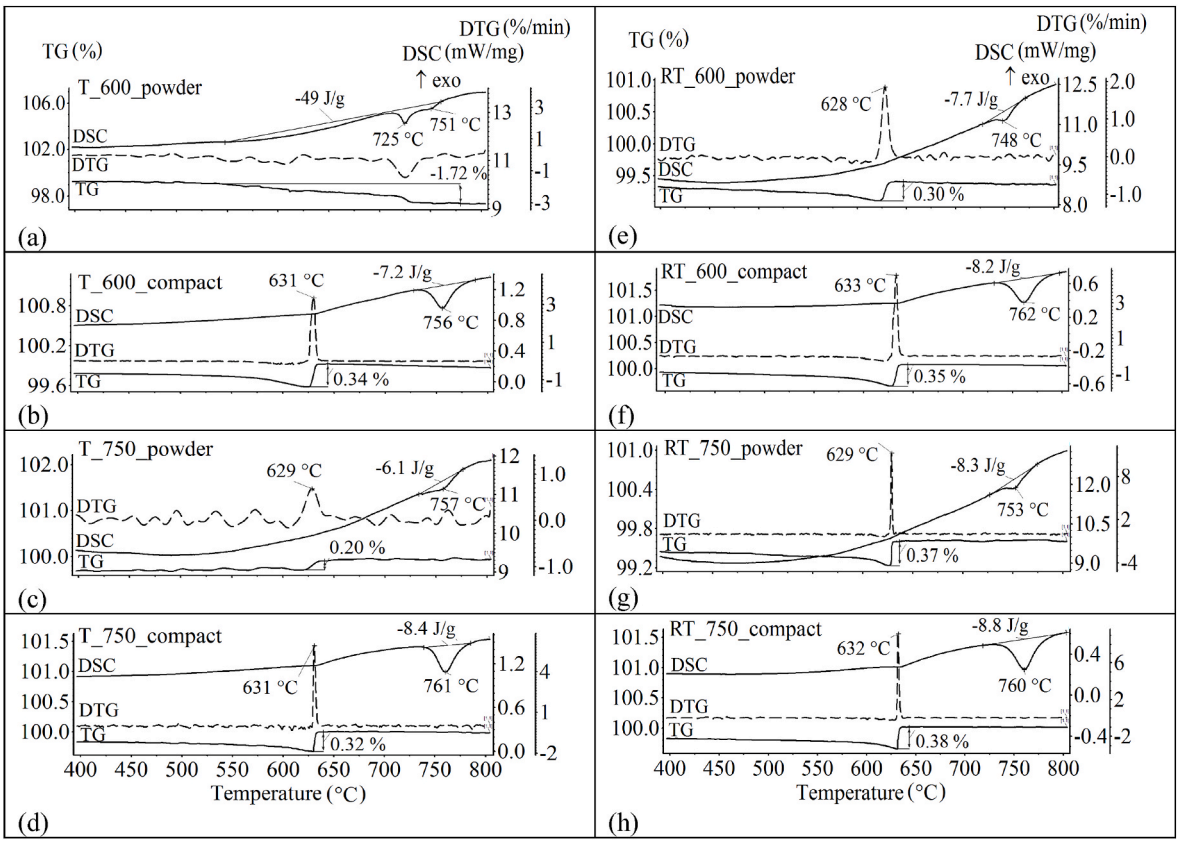

Fig. 8. TG/DSC analysis performed under heating of Li ferrite samples synthesized at 600 °C and 750 °C from powder and compact.

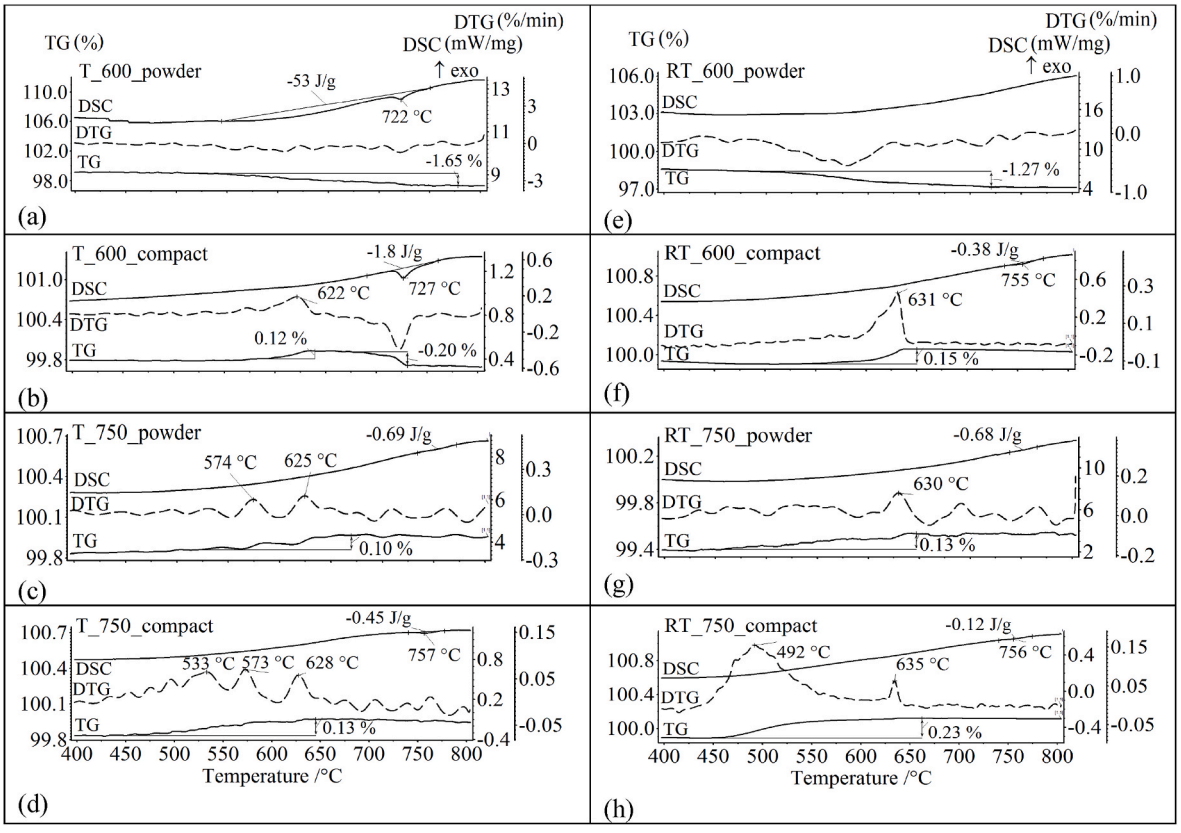

Fig. 9. TG/DSC analysis performed under heating of Li–Zn ferrite samples synthesized at 600 °C and 750 °C from powder and compact.

reagents.

CRediT authorship contribution statement

Elena N. Lysenko: Investigation, Methodology, Formal analysis, Writing – original draft. **Vitaly A. Vlasov:** Validation, Data curation. **Evgeniy V. Nikolaev:** Data curation, Software. **Anatoliy P. Surzhikov:** Conceptualization, Funding acquisition, Project administration, Supervision. **Mikhail V. Korobeynikov:** Writing – review & editing, All authors have read and agreed to the published version of the manuscript.

Declaration of competing interest

The authors declare that they have no known competing financial interests or personal relationships that could have appeared to influence the work reported in this paper.

Data availability

Data will be made available on request.

Acknowledgements

This work was supported by the Russian Science Foundation under grant No. 22-19-00183.

References

[1] Ü. Özgür, Y. Alivov, H. Morkoç, Microwave ferrites, part 1: fundamental properties, J. Mater. Sci. Mater. Electron. 20 (2009) 789–834, https://doi.org/10.1007/s10854-009-9923-2.
[2] A. Goldman, Modern Ferrite Technology, Springer, 2006, https://doi.org/10.1007/978-0-387-29413-1_11.
[3] Sandeep B. Somvanshi, Swapnil A. Jadhav, Mangesh V. Khedkar, Prashant B. Kharat, S.D. More, K.M. Jadhav, Structural, thermal, spectral, optical and surface analysis of rare earth metal ion (Gd^{3+}) doped mixed Zn–Mg nano-spinel ferrites, Ceram. Int. 46 (2020) 13170–13179, https://doi.org/10.1016/j.ceramint.2020.02.091.
[4] Sandeep B. Somvanshi, Mangesh V. Khedkar, Prashant B. Kharat, K.M. Jadhav, Influential diamagnetic magnesium (Mg^{2+}) ion substitution in nano-spinel zinc ferrite ($ZnFe_2O_4$): thermal, structural, spectral, optical and physisorption analysis, Ceram. Int. 46 (2020) 8640–8650, https://doi.org/10.1016/j.ceramint.2019.12.097.
[5] A.V. Anupama, V. Rathod, V.M. Jali, B. Sahoo, Composition dependent elastic and thermal properties of Li-Zn ferrites, J. Alloys Compd. 728 (2017) 1091–1100. https://doi:10.1016/j.jallcom.2017.09.099.
[6] M.S. Ruiz, S.E. Jacobo, Electromagnetic properties of lithium zinc ferrites doped with aluminum, Physica B 407 (2012) 3274–3277. https://doi:10.1016/j.physb.2011.12.085.
[7] N.I. Abu-Elsaad, S.A. Mazen, H.M. Salem, The effect of zinc substitution and heat treatment on microstructural and magnetic properties of Li ferrite nanoparticles, J. Alloys Compd. 835 (2020), 155227. https://doi:10.1016/j.jallcom.2020.155227.
[8] M. Mahmoudi, M. Kavanlouei, Temperature and frequency dependence of electromagnetic properties of sintering Li–Zn ferrites with nano SiO_2 additive, J. Magn. Magn Mater. 384 (2015) 276–283. https://doi:10.1016/j.jmmm.2015.02.053.
[9] I.M. Isaev, V.G. Kostishin, V.V. Korovushkin, D.V. Salogub, R.I. Shakirzyanov, A. V. Timofeev, A.Yu Mironovich, Magnetic and radio-absorbing properties of polycrystalline $Li_{0.33}Fe_{2.29}Zn_{0.21}Mn_{0.17}O_4$ spinel ferrite, Tech. Phys. 66 (2021) 1216–1220, https://doi.org/10.1134/S1063784221090085.
[10] C.E. Patton, C.A. Edmondson, Y.H. Liu, Magnetic properties of lithium zinc ferrite, J. Appl. Phys. 53 (1982) 2431–2433, https://doi.org/10.1063/1.330835.
[11] V. Rathod, A.V. Anupama, V.M. Jali, V.A. Hiremath, B. Sahoo, Combustion synthesis, structure and magnetic properties of Li-Zn ferrite ceramic powders, Ceram. Int. 43 (2017) 14431–14440. https://doi:10.1016/j.ceramint.2017.07.213.
[12] V. Rathod, A.V. Anupama, R. Vijaya Kumar, V.M. Jali, B. Sahoo, Correlated vibrations of the tetrahedral and octahedral complexes and splitting of the absorption bands in FTIR spectra of Li-Zn ferrites, Vib. Spectrosc. 92 (2017) 267–272. https://doi:10.1016/j.vibspec.2017.08.008.
[13] A. Manzoor, M. Azhar Khan, M. Yaqoob Khan, M. Niaz Akhtar, A. Hussain, Tuning magnetic and high frequency dielectric behavior in Li-Zn ferrites by Ho doping, Ceram. Int. 44 (2018) 6321–6329. https://doi:10.1016/j.ceramint.2018.01.022.
[14] G. Yuheng, Z. Jianguo, L. Haiyan, Study on structure, magnetic and dielectric properties of Li-Zn ferrite with low ferromagnetic resonance line-width and high saturation magnetization synthesized at low temperature by LTCC, Ceram. Int. 47 (2021) 9111–9117. https://doi:10.1016/j.ceramint.2020.12.034.
[15] S.E. Shirsath, D. Wang, S.S. Jadhav, M.L. Mane, S. Li, Ferrites obtained by sol-gel method, in: L. Klein, M. Aparicio, A. Jitianu (Eds.), Handbook of Sol-Gel Science and Technology, Springer, Cham, 2018, https://doi.org/10.1007/978-3-319-32101-1_125.
[16] P.V. Bhasker Reddy, B. Ramesh, Ch Gopal Reddy, Electrical conductivity and dielectric properties of zinc substituted lithium ferrites prepared by sol–gel method, Physica B 405 (2010) 1852–1856. https://doi:10.1016/j.physb.2010.01.062.
[17] G. Yu, W. Zhi, Microwave absorption and electromagnetic interference shielding properties of Li-Zn ferrite-carbon nanotubes composite, J. Magn. Magn Mater. 528 (2021), 167808. https://doi:10.1016/j.jmmm.2021.167808.
[18] K. Naz, J.K. Khan, M. Khalid, M.S. Akhtar, Z.A. Gilani, H.M. Noor ul Huda Khan Asghar, Gaber A.M. Mersal, Mohamed M. Ibrahim, A. Muhammad, M.G.B. Ashiq, Structural, dielectric, impedance and electric modulus analysis of Ni substituted copper spinel ferrites nanoparticles for microwave device applications, Mater. Chem. Phys. 285 (2022), 126091, https://doi.org/10.1016/j.matchemphys.2022.126091.
[19] S. Kotru, R. Paul, A.Q. Jaber, Synthesis and magnetic studies of pure and doped NiZn ferrite films using Sol gel method, Mater. Chem. Phys. 276 (2022), 125357, https://doi.org/10.1016/j.matchemphys.2021.125357.
[20] Q. Khan, A. Majeed, N. Ahmad, I. Ahmad, R. Ahmad, Structural features and dielectric behavior of Al substituted $Cu_{0.7}Ni_{0.3}Fe_2O_4$ ferrites, Mater. Chem. Phys. 273 (2021), 125028, https://doi.org/10.1016/j.matchemphys.2021.125028.
[21] N.I. Abu-Elsaad, S.A. Mazen, A.Y. Sleem, Production of Cr^{3+} substituted Li–Zn nanocrystalline ferrite by citrate method: studies on structure, cation occupancy, elastic, optical and magnetic performance, Ceram. Int. 48 (2022) 14210–14223.
[22] A. Subha, M.G. Shalini, B.N. Sahu, S. Rout, Subasa C. Sahoo, Role of surface defects and anisotropy variation on magnetic properties of copper ferrite nanoparticles prepared by co-precipitation method, Mater. Chem. Phys. 286 (2022), 126212, https://doi.org/10.1016/j.matchemphys.2022.126212.
[23] S. Solyman, H.M. Zaki, S. Soliman, Investigation of structural, magnetic and electrical properties of aluminum substituted Co-Mg ferrite, Mater. Chem. Phys. 279 (2022), 125723, https://doi.org/10.1016/j.matchemphys.2022.125723.
[24] P.V.V. Romanholo, T.E.P. Alves, J. Swapnalin, P. Banerjee, A. Franco, Tailoring the magnetic properties of Zn doped nickel, magnesium and cobalt ferrite ceramics, Mater. Chem. Phys. 284 (2022), 126072, https://doi.org/10.1016/j.matchemphys.2022.126072.
[25] U.B. Gawas, V.M.S. Verenkar, V.T. Vader, Anil Jain, Sher Singh Meena, Effects of sintering temperature on microstructure, initial permeability and electric behaviour of Ni-Mn-Zn ferrites, Mater. Chem. Phys. 275 (2022), 125250, https://doi.org/10.1016/j.matchemphys.2021.125250.
[26] Q. Yang, H. Zhang, Q. Wen, Y. Liu, X. Yang, Magnetic properties of lithium zinc ferrites synthesized by microwave sintered method, AIP Adv. 6 (2016), 055936, https://doi.org/10.1063/1.4946899.
[27] B. Chacko, A. Roy, A.M. Richard, J. Swathy, B.T. Avanish, W. Madhuri, Bismuth modified zinc ferrites for low-temperature ceramic co-firing technology, Mater. Chem. Phys. 276 (2022), 125401, https://doi.org/10.1016/j.matchemphys.2021.125401.
[28] A.A. Sattar, H.M. El-Sayed, W.R. Agami, A.A. Ghani, Magnetic properties and electrical resistivity of Zr^{4+} substituted Li-Zn ferrite, Am. J. Appl. Sci. 4 (2) (2007) 89–93. https://doi:10.3844/AJASSP.2007.89.93.
[29] P. Kumar Dipti, J.K. Juneja, S. Singh, K.K. Raina, C. Prakash, Improved dielectric and magnetic properties in modified lithium-ferrites, Ceram. Int. 41 (2015) 3293–3297. https://doi:10.1016/j.ceramint.2014.10.092.
[30] P. Kumar, J.K. Juneja, C. Prakash, S. Singh, R.K. Shukla, K.K. Raina, High DC resistivity in microwave sintered $Li_{0.49}Zn_{0.02}Mn_{0.06}Fe_{2.43}O_4$ ferrites, Ceram. Int. 40 (2014) 2501–2504. https://doi:10.1016/j.ceramint.2013.07.063.
[31] L. Jia, Y. Zhao, F. Xie, Q. Li, Y. Li, C. Liu, H. Zhang, Composition, microstructures and ferrimagnetic properties of Bi-modified LiZnTiMn ferrites for LTCC, AIP Adv. 6 (2016), 056214. https://doi:10.1063/1.4943928.
[32] U.V. Ancharova, M.A. Mikhailenko, B.P. Tolochko, N.Z. Lyakhov, M. V. Korobeinikov, A.A. Bryazgin, V.V. Bezuglov, E.A. Shtarklev, Synthesis and staging of the phase formation for strontium ferrites in thermal and radiation thermal reactions, IOP Conf. Ser. Mater. Sci. Eng. 81 (2015), 012122. https://doi:10.1088/1757-899X/81/1/012122.
[33] V.A. Zhuravlev, E.P. Naiden, R.V. Minin, V.I. Itin, V.I. Suslyaev, E.Yu Korovin, Radiation-thermal synthesis of W-type hexaferrites, IOP Conf. Ser. Mater. Sci. Eng. 81 (2015), 012003. https://doi:10.1088/1757-899X/81/1/012003.
[34] V.G. Kostishin, R.I. Shakirzyanov, A.G. Nalogin, S.V. Shcherbakov, I.M. Isaev, M. A. Nemirovich, M.A. Mikhailenko, M.V. Korobeinikov, M.P. Mezentseva, D. V. Salogub, Electrical and dielectric properties of yttrium–iron ferrite garnet polycrystals grown by the radiation–thermal sintering technology, Phys. Solid State 63 (3) (2021) 435–441. https://doi: 10.1134/S1063783421030094.
[35] V.G. Kostishin, V.G. Andreev, V.V. Korovushkin, D.N. Chitanov, N.A. Yudanov, A. T. Morchenko, A.S. Komlev, A.Yu Adamtsov, A.N. Nikolaev, Preparation of 2000NN ferrite ceramics by a complete and a short radiation-enhanced thermal sintering process, Inorg. Mater. 50 (2014) 1317. https://doi:10.1134/S0020168514110089.
[36] V.G. Kostishin, V.V. Korovushkin, A.G. Nalogin, S.V. Shcherbakov, I. Isaev, A. A. Alekseev, A.Yu Mironovich, D. Salogub, Features of the magnetic structure of Y3Fe5O12 polycrystals synthesized by radiation thermal sintering, Phys. Solid State 62 (2020) 1156. https://doi:10.1134/S1063783420070124.
[37] E.N. Lysenko, V.A. Vlasov, A.P. Surzhikov, A.I. Kupchishin, Kinetic study of lithium–zinc ferrite synthesis under electron beam heating conditions, Inorg. Mater. Appl. Res. 13 (2022) 494–500. https://doi:10.1134/S2075113322020265.

[38] E.N. Lysenko, V.A. Vlasov, A.P. Surzhikov, Investigation of kinetics of lithium ferrite formation under electron beam treatment, Nucl. Instrum. Methods Phys. Res. Sect. B Beam Interact. Mater. Atoms 466 (2020) 31–36. https://doi: 10.1016/j.nimb.2020.01.010.
[39] M.E. Brown, P.K. Gallagher, Handbook of Thermal Analysis and Calorimetry, Elsevier Science B.V., 2008. https://doi:10.1016/S1573-4374(13)60004-7.
[40] P.K. Gallagher, Thermomagnetometry, J. Therm. Anal. Calorim. 49 (1997) 33–44. https://doi:10.1007/BF01987419.
[41] D.M. Lin, H.S. Wang, M.L. Lin, M.H. Lin, Y.C. Wu, TG(M) and DTG(M) techniques and some of their applications on material study, J. Therm. Anal. Calorim. 58 (1999) 347–353. https://doi:10.1023/A:1010199004211.
[42] A.L. Astafyev, E.N. Lysenko, A.P. Surzhikov, Thermomagnetometric analysis of lithium ferrites, J. Therm. Anal. Calorim. 136 (2019) 441–445. https://doi:10.1007/s10973-018-7678-9.
[43] E.N. Lysenko, E.V. Nikolaev, V.A. Vlasov, A.P. Surzhikov, Microstructure and reactivity of Fe2O3-Li2CO3-ZnO ferrite system ball-milled in a planetary mill, Thermochim. Acta 664 (2018) 100–107. https://doi:10.1016/j.tca.2018.04.015.
[44] V. Verma, V. Pandey, S. Singh, R.P. Aloysius, S. Annapoorni, R.K. Kotanala, Comparative study of structural and magnetic properties of nano-crystalline $Li_{0.5}Fe_{2.5}O_4$ prepared by various methods, Physica B 404 (2009) 2309–2314. https://doi:10.1016/j.physb.2009.04.034.
[45] S.H. Gee, Y.K. Hong, M.H. Park, D.W. Erickson, P.J. Lamb, Synthesis of nanosized $(Li_{0.5x}Fe_{0.5x}Zn_{1-x})Fe_2O_4$ particles and magnetic properties, J. Appl. Phys. 91 (2002) 7586–7588, https://doi.org/10.1063/1.1453931.
[46] E.N. Lysenko, E.V. Nikolaev, A.P. Surzhikov, S.A. Nikolaeva, I.V. Plotnikova, The influence of reagents ball milling on the lithium ferrite formation, J. Therm. Anal. Calorim. 138 (2019) 2005–2013. https://doi: 10.1007/s10973-019-08334-1.
[47] V. Berbenni, A. Marini, P. Matteazzi, R. Ricceri, N.J. Welham, Solid-state formation of lithium ferrites from mechanically activated Li_2CO_3 – Fe_2O_3 mixtures, J. Eur. Ceram. Soc. 23 (2003) 527–536. https://doi:10.1016/S0955-2219(02)00150-4.
[48] S.Y. An, I.-B. Shim, C.S. Kim, Synthesis and magnetic properties of LiFe5O8 powders by a sol–gel process, J. Magn. Magn Mater. 290–291 (2005) 1551–1554. https://doi:10.1016/j.jmmm.2004.11.244.
[49] E. Lysenko, A. Malyshev, V. Vlasov, E. Nikolaev, A. Surzhikov, Microstructure and thermal analysis of lithium ferrite pre-milled in a high energy ball mill, J. Therm. Anal. Calorim. 134 (2018) 127–133. https://doi: 10.1007/s10973-018-7549-4.
[50] E.N. Lysenko, A.P. Surzhikov, A.V. Malyshev, V.A. Vlasov, E.V. Nikolaev, Thermal analysis study of solid-phase synthesis of zinc- and titanium-substituted lithium ferrites from mechanically activated reagents, J. Therm. Anal. Calorim. 122 (2015) 1347–1353. https://doi:10.1007/s10973-015-4849-9.
[51] J.M.F. Lucas, P.R. Prezas, S.S. Teixeira, N.M. Ferreira, A.J.M. Sales, B.M.G. Melo, M.P.F. Graça, Tuning the magnetic and electric behavior of lithium ferrite using an eco-friendly pectin sol-gel route, J. Sol. Gel Sci. Technol. 98 (2021) 580. https://doi:10.1007/s10971-021-05513-1.
[52] M.M. Hessien, Synthesis and characterization of lithium ferrite by oxalate precursor route, J. Magn. Magn Mater. 320 (2008) 2800–2807. https://doi:10.1016/j.jmmm.2008.06.018.